Check for updates

Journal of
Materials Chemistry A

Accepted Manuscript

Journal of
Materials Chemistry A

Materials for energy and sustainability
www.rsc.org/MaterialsA

Volume 4 | Number 1 | 7 January 2016 | Pages 1–330

ROYAL SOCIETY
OF CHEMISTRY

PAPER
Kun Chang, Zhaorong Chang et al.
Bubble-template-assisted synthesis of hollow fullerene-like
MoS₂ nanocages as a lithium ion battery anode material

ISSN 2050-7488

175 YEARS

ROYAL SOCIETY
OF CHEMISTRY

rsc.li/materials-a

ROYAL SOCIETY
OF CHEMISTRY

Journal Name

ARTICLE

Tuning the Selectivity of Light Hydrocarbons in Natural Gas in a Family of Isoreticular MOFs

Thais Grancha,[a] Marta Mon,[a] Jesús Ferrando-Soria,*[a] Jorge Gascon,[b] Beatriz Seoane,[b] Enrique V. Ramos-Fernandez,[c] Donatella Armentano,*[d] and Emilio Pardo*[a]

Purification of methane from other light hydrocarbons in natural gas is a topic of intense research due to its fundamental importance in the utilization of natural gas fields. Porous materials have emerged as excellent alternative platforms to conventional cryogenic methodologies to perform this task in a cost- and energy-efficient manner. Here we report a new family of isoreticular chiral MOFs, prepared from oxamidato ligands derived from the natural amino acids L-alanine, L-valine and L-leucine, where, by increasing the length of the alkyl residue of the amino acid, the charge density of the MOF's channels can be tuned (**1** > **2** > **3**), decreasing the adsorption preference towards methane over light hydrocarbons thus improving this purification process. The validity of our rational design strategy has been proved by a combination of single-component adsorption isotherms, adsorption kinetics of CH_4, C_2H_6, C_3H_8 and n-C_4H_{10}, and breakthrough experiments of binary CH_4/C_2H_6 and CH_4/C_3H_8 mixtures.

Introduction

Light hydrocarbons, C_1–C_4, are a basic feedstock for the chemical industry, generally obtained through steam cracking, but also present in natural gas and other less conventional gas fields.[1] The separation of the different light hydrocarbons present in natural gas is particular important from industrial and ecological viewpoints.[2] In fact, the upgrading of natural gas is mandatory in order to fully exploit the highly abundant methane gas.[3] Currently, the purification of methane from the other light hydrocarbons in natural gas is performed by cryogenic liquefaction and fractional distillation, which represents the most cost- and energy-demanding step on the production of these important chemicals.[4] Hence, the development of new energy-efficient separation methodologies is highly desirable. Among the latest advances on implementing separation technologies,[5] adsorption on porous materials has emerged as a strong alternative to overcome the current energy penalties associated to the purification process of light hydrocarbons.[6]

Metal-Organic Frameworks (MOFs)[7–12] are a class of porous materials that provide countless applications in many fields due to the myriad of thrilling physical properties[13,14] they can offer, which are mainly associated to their porous character and rich host-guest chemistry.[15] However, in order to have the desired property in a MOF, it is mandatory an accurate control of the MOF structure, and more precisely, of the size, shape and functionalization of the channels of the porous network.[16–20] In this context, even if a total control of the structure is a challenge because of the many subtle factors that may affect the assembling process,[21] MOFs with predetermined dimensionalities and specific topologies[22,23] can somehow be designed by a careful choice of metal ions and design of the organic ligands. In addition, due to their crystalline nature, X-ray crystallography allows to shed light and precisely determine their crystal structure and accordingly establish structure-property relationships, which can be hardly done in other porous systems and explains the burgeoning growth of MOFs.[24,25]

Among the tuneable physical properties of MOFs, those regarding the adsorption-based phenomena, such as gas adsorption[26,27] and separation[28,29] have attracted a lot of attention due to the global interest to move towards green economy and sustainable industrial development.[28,29] The former point can include the removal of non-desired species like toxic[30,31] and green-house[32–34] gases or the purification of the desired hydrocarbon.[35–46] In particular, the most appealing strategies towards MOF-driven gas separation of light hydrocarbons consist either on a conscious design effort[46] or on the application of a post-synthetic methodology[47] in order to gain control and tune the size, shape and functionality of the MOF's void channels.[16] Through these strategies, which rely on kinetic-based and/or thermodynamic-based mechanisms as well as on particular structural features, such as interpenetration or gate-opening effects, interesting light hydrocarbons separations have been performed.[48]

[a] Instituto de Ciencia Molecular (ICMOL), Universidad de Valencia, 46980 Paterna, Valencia, Spain. E-mail: jesus.ferrando@uv.es (J.F-S.), Emilio.Pardo@uv.es (E.P.)
[b] Catalysis Engineering-Chemical Engineering Dept., Delft University of Technology, Julianalaan 136, 2628 BL Delft, The Netherlands
[c] Laboratorio de Materiales Avanzados, Departamento de Química Inorgánica-Instituto Universitario de Materiales, Universidad de Alicante, Alicante, Spain.
[d] Dipartimento di Chimica e Tecnologie Chimiche, Università della Calabria, 87036 Rende, Cosenza, Italy. E-mail: Donatella.armentano@unical.it

We show here the use of a rationally programmed method to build a new family of isoreticular MOFs,[49] consisting on the use of metalloligands with increasing length of their alkyl substituents. This method offers the possibility to finely tune the charge density of the MOF channels, by the concomitant pore size reduction and increase in the number of aliphatic residues, tailoring the kinetic adsorption selectivity of methane towards other light hydrocarbons present in natural gas.[16–20] Thus, as a part of our recent research concerning the use of chiral oxamidato ligands derived from natural amino acids,[23,50–53] we report here the synthesis, crystal structures and gas sorption properties of a novel family of water-stable isoreticular chiral *bio*MOFs of general formula {$Ca^{II}Cu^{II}_6L_3(OH)_2(H_2O)$} · nH_2O [**1**[51]: L = (*S,S*)-alamox = [bis[(*L*)-alanine]oxalyl diamide] (*n* = 32); **2**: L = (*S,S*)-valmox = [bis[(*L*)-valine]oxalyl diamide] (*n* = 13) and **3**: L = (*S,S*)-leumox = [bis[(*L*)-leucine]oxalyl diamide] (*n* = 11)] (see Scheme 1). These materials show very different gas sorption properties depending on the size of the aliphatic residue of the amino acid-based ligand (Scheme 1), which allows an exquisite control of the hydrophobicity of the channels and thus of the kinetic adsorption selectivity of methane from other components of natural gas.
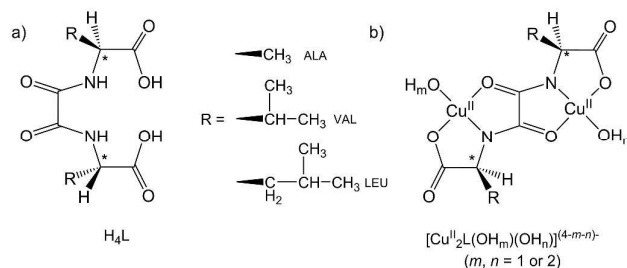
Scheme 1. (a) Chemical structures of the chiral bis(amino acid)oxalamide ligands emphasizing the increasing size of the amino acid residue in the series alanine, valine, leucine and (b) the corresponding dianionic bis(hydroxo)dicopper(II) complexes.

Results and Discussion

Preparation and X-ray Crystal Structure

2 and **3** were prepared as reported earlier for **1**.[51] Slow diffusion of aqueous solutions of the corresponding bis(hydroxo)dicopper(II) complex precursor, $(NMe_4)_2${$Cu_2L(OH)_2$} · nH_2O, and $CaCl_2$ · $4H_2O$ (3:1 molar ratio) in a H-shaped tube at room temperature yielded blue/green elongated hexagonal prisms in all cases (see ESI†).

The structures of **2** and **3** could be also determined by X-ray diffraction on single crystals. **1–3** are isomorphous and crystallize in the chiral $P6_3$ space group of the hexagonal system (Table S1). Their structures can be described as chiral 3D calcium(II)-copper(II) networks with a uni-nodal six-connected **acs** net,[54,55] with point symbol of ($4^9.6^6$). Within the networks, the dicopper units, [$Cu^{II}_2L(OH)_2$], connect the Ca^{II} ions through their carboxylate groups. Three aqua/hydroxo molecules (with 1:2 statistical distribution) coordinated in a μ_3 fashion, are also involved (Figs. 1 and S1-S2). As a result, the Ca^{II} ions are nona-coordinated in a distorted monocapped square antiprism geometry.

The 3D $Ca^{II}Cu^{II}_6$ networks in **1-3**, exhibit a honeycomb-like hexagonal architecture, giving rise to relatively large hexagonal channels along the *c* axis (Fig. 2). The Ca^{II} ions occupy the vertices of

each hexagonal channel, the adjacent Ca···Ca distance, constituting the edge of each ring, being of 12.187(1), 12.122(4) and 12.076(4) Å for **1**-**3**, respectively. In turn, the square pyramidal or square Cu^{II} ions situate along the edges of the channels (Figs. 2 and S1).
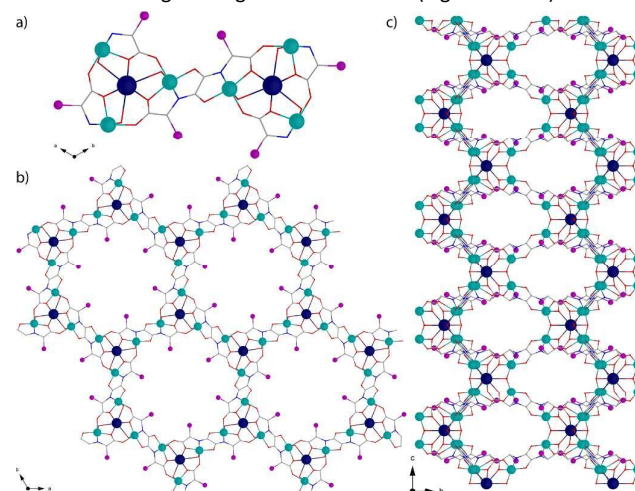

Fig. 1. a) Common dicopper(II) building blocks in **1**-**3**. Views of **1**-**3** in the *ab* (b) and *bc* (c) planes, respectively. Copper and calcium atoms are represented by cyan and blue spheres, respectively, whereas the ligands are depicted as sticks (carbon: grey, oxygen: red and nitrogen: blue). The purple spheres represent the amino acid residues (see Scheme 1).

The most striking structural feature of this series of isoreticular compounds arises from the orientation of the amino acid residues pointing inwards the hexagonal channels and interstitial voids (Figs. 2, bottom and S1, S3-S8). Methyl groups in **1** and isopropyl chains in **2** both show a medium to regular distended conformation. In contrast, only one of the two isobutyl residues exhibits a distended conformation inwards the pores in **3** (Fig. S2). Leucine residues being more hydrophobic and longer and so more hindered than others, most likely prefer to be buried in large space to reach the more stable folding, forcing one of the flexible isobutyl chains to adopt a highly bent conformation with their methyl groups pointing outward the pores (Fig. S2c). For a structure-properties relationship might be of interest to underline that the great framework flexibility, verified in particular in the longer amino acid side chains isopropyl (**2**) and isobutyl (**3**), undoubtedly will influence the diffusion of gases in the pores. Thus, it must be one of the synergic factors to take into account when aiming at achieving a fine control on the selectivity and separation of, for example, methane in natural gas. In particular, the X-ray structure reveals a high thermal motion of the carbon atoms belonging to the leucine amino acid residues in **3**. This is enough to suppose a further optimization of the more stable side-chains conformation, thus enhancing efficient host-guest interactions or allowing also opportunistic hopping of these gases along the pores.

Because of the different size of the hydrophobic methyl (**1**), isopropyl (**2**) and isobutyl (**3**) groups, the resulting channels possess varying virtual diameters of *ca.* 1.0 (**1**), 0.75 (**2**) and 0.5 (**3**) nm (Figs. S3-S8). Hence, in a static view, the pore-limiting diameters from the crystal structures are large enough to permit, in principle, the diffusion of different light hydrocarbons (*vide infra*) such as methane (CH_4), ethane (C_2H_6), ethylene (C_2H_4), propane (C_3H_8),

Journal Name

ARTICLE

propylene (C_3H_6) and butane ($n\text{-}C_4H_{10}$) which have related estimated kinetic diameters increasing from 3.8 Å for CH_4 up to 4.7 Å for $n\text{-}C_4H_{10}$.[28] The increasing degree of hydrophobicity together with the decreasing size of the pores account for the contents of free water molecules [32 (**1**), 13 (**2**) and 11 (**3**)]. This increasing charge density at the channels from **1** to **3** also suggest different

functionality of the channels and is reflected in the gas adsorption of light hydrocarbons (see below). Finally, the estimated empty volumes for **1-3** without the crystallization water molecules is 2089.1 (**1**), 1532.6 (**2**) and 1312.0 (**3**) Å^3, values which represent *ca.* 58.0, 43.4 and 37.5 %, respectively, of potential void per unit cell volume [V = 3604.1 (**1**), 3529.7 (**2**) and 3501.0 (**3**) Å^3] (Figs. S3-S8).
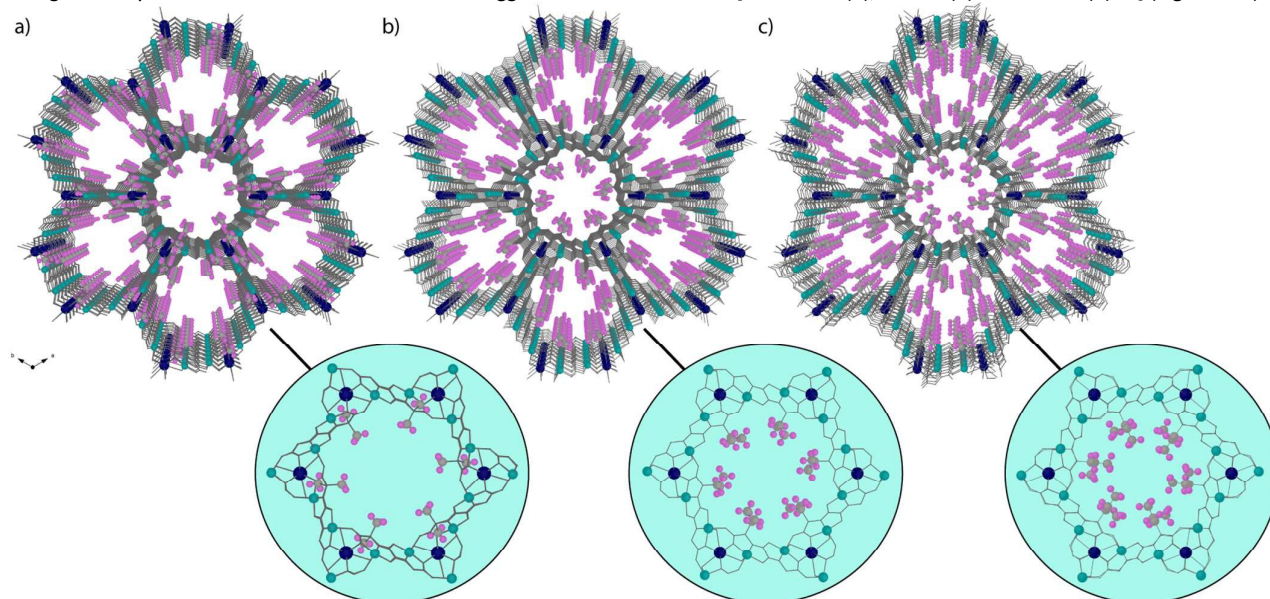

Fig. 2. (a) Perspective views along the crystallographic *c* axis of the porous structures of **1** (a), **2** (b) and **3** (c), determined by single-crystal X-ray diffraction, emphasizing the different alkyl groups in the boxed structures. Copper and calcium atoms are represented by cyan and blue spheres, respectively. The alkyl residues of the amino acids are shown as balls and sticks whereas the remaining carbon, nitrogen and oxygen atoms from the ligand are shown as sticks. Free water solvent molecules are omitted for clarity.

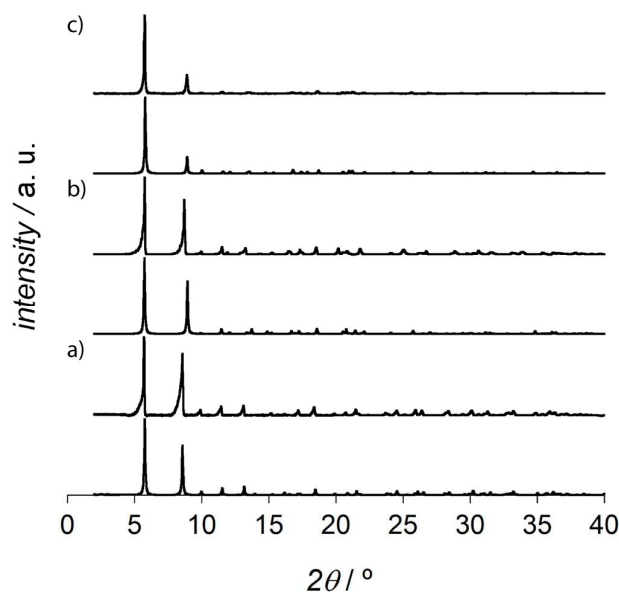## Thermogravimetric Analysis and X-Ray Powder Diffraction

Fig. 3. Calculated (bottom) and experimental (top) XRPD pattern profiles of polycrystalline samples of **1** (a), **2** (b) and **3** (c) measured in the 2ϑ range 2.0–40.0° at r.t.

The thermogravimetric analyses (TGA) under dry N_2 atmosphere indicated the water contents of **1-3** (Fig. S9). The mass

loss values of *ca.* 31.5 (**1**), 15 (**2**), and 12% (**3**) at 150 °C are consistent with 32, 13, and 11 H_2O molecules per formula unit, respectively. Even if the larger pores in **1** undoubtedly influence the very large number of water molecules that its channels can accommodate, these results already suggest the very different hydrophobicity of the members of the family. Therefore, the number of crystallization water molecules filling the pores of **2** and **3** is drastically reduced compared to **1** as a consequence of their much larger alkyl chains and the resulting more hydrophobic environment.

The powder X-ray diffraction (PXRD) patterns of polycrystalline samples of **1-3** at room temperature (Fig. 3) confirm the pureness of the bulk samples with a consistent match between the experimental and calculated PXRD patterns.

Gas Sorption Properties

All samples of **1-3** were activated by immersion in methanol and then desolvated at 80 °C under reduced pressure for 24 h prior to the sorption measurements. Nitrogen adsorption isotherms at 77 K for **1-3** (Fig. 4) show fully reversible type I isotherms, characteristic of microporous materials with permanent microporosity, with estimated[56] Brunauer–Emmett–Teller (BET) surface areas [1015 (**1**), 561 (**2**), and 312 m^2/g (**3**)] following the trend **1 > 2 > 3**, as expected from their decreasing pore size (estimated from the crystal structures). The analyses of the N_2 isotherm curves using the Horvath-Kawazoe model,[57] reveal a microporous

Journal of Materials Chemistry A Accepted Manuscript

ARTICLE

Journal Name

pore size distribution for **1**-**3** [1.08 (**1**), 0.68 (**2**), and 0.42 nm (**3**)], which are similar to those determined from the crystal structure and preclude to assign the slight increase near saturation pressure to mesoporosity or N_2 condensation in the inter-particle space. In turn, it has been attributed to capillary condensation. The same behaviour was observed for the CO_2 adsorption isotherms, with a decrease in the gas uptake at 1 bar and 273 K [106.0 (**1**), 44.1 (**2**), and 22.3 cm^3/g (**3**)] with increasing the length of the amino acid residue (Fig. S10).
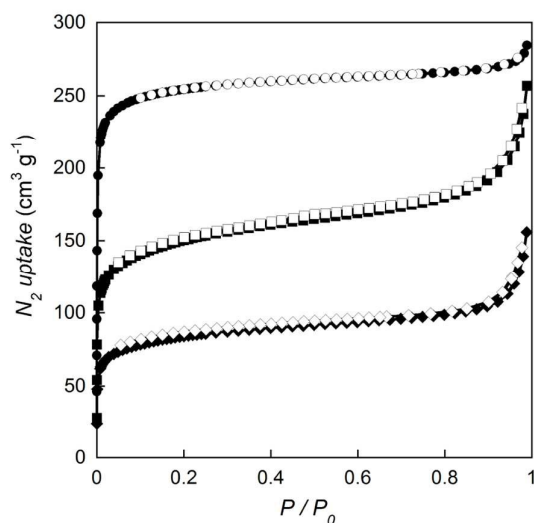

Fig. 4. N_2 sorption isotherms for the activated compounds **1** (○), **2** ( ) and **3** (◊) at 77 K. Filled and empty symbols indicate the adsorption and desorption isotherms respectively.

Once demonstrated the permanent microporosity of **1**-**3** as well as their different pore windows depending on the amino
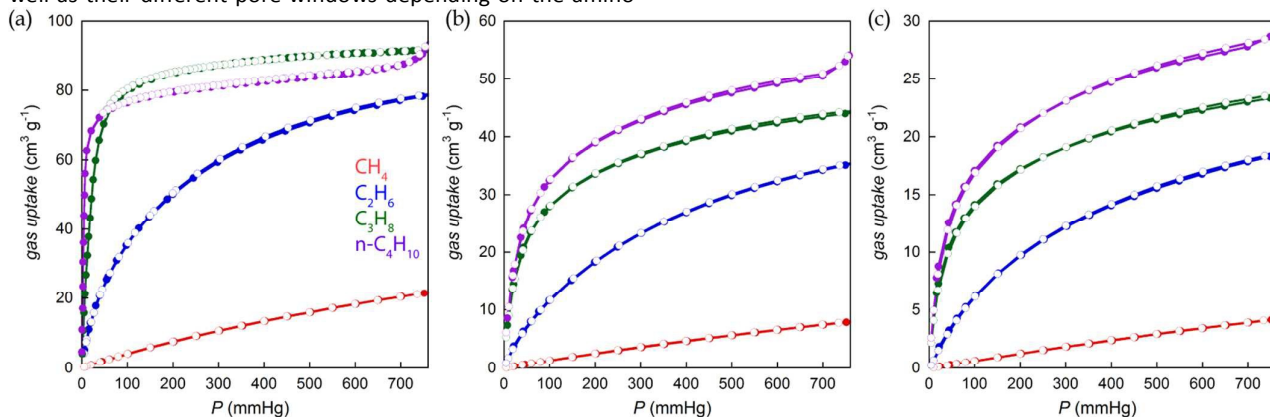
acid residue filling the cavities, we studied the performance of this family in the adsorption of different light hydrocarbons such as methane (CH_4), ethane (C_2H_6), ethylene (C_2H_4), propane (C_3H_8), propylene (C_3H_6) and butane (n-C_4H_{10}). So far, several adsorption studies have been carried out, for different MOFs, aiming at evaluating the adsorptive properties towards different olefins and paraffins.[35–46] This is commonly done by measuring single-component adsorption isotherms, as well as simulating mixed gas adsorption isotherms with the ideal adsorbed solution theory[58] or transient breakthrough[59] and/or, less frequently, by performing breakthrough experiments.[43,45,60–66] In particular, relevant to our study are the different reported MOFs performing separation of CH_4 from C_2, C_3 or C_4 hydrocarbons.[43,45,60–66] In these studies, they use bulky aromatic groups,[45] nitrogen donor moieties[43,65] and pendant C_3 alkoxy groups with various degrees of branching and saturation,[67] and/or coordinatively unsaturated metal sites[62] to increase the charge density of the channels, and consequently increase the interaction of C_{2+} hydrocarbons with the MOF's pores. However, **1**-**3** offer unique possibilities towards evaluating the real impact of the length of the alkyl side-chains occupying the channels in the adsorption of different light hydrocarbons. Indeed, this is the first experimental study in which a family of isoreticular MOFs exhibiting different alkyl-functionalized pores is used to rationalize these adsorptive properties. Thus, the systematic variation of the length of the aliphatic residue will allow us to evaluate at the same time the influence of different parameters such as the pore window, hydrophobicity, kinetics and alkyl interactions in the adsorption, and consequently the selectivity towards light hydrocarbons in **1**-**3**.

Fig. 5. CH_4 (red), C_2H_6 (blue), C_3H_8 (green) and C_4H_{10} (purple) adsorption isotherms for **1** (a), **2** (b), and **3** (c) at 273 K. Filled and empty symbols indicate the adsorption and desorption isotherms respectively.

Therefore, adsorption isotherms of light paraffins, CH_4, C_2H_6, C_3H_8 and n-C_4H_{10}, were firstly measured for **1**-**3** up to 1 bar at 273 K (Fig. 5). The adsorption capacities at 1 bar follow the same trend for **1**-**3**. An increase with the carbon chain length was observed, following the sequence CH_4 << C_2H_6 < C_3H_8 < n-C_4H_{10}, as result of the enhancement of interactions

with the side chain of the MOF. The only exception is for n-C_4H_{10} in compound **1**, which adsorbs a slightly higher C_3H_8 amount at 1 bar. This could be related to a less efficient packing of n-C_4H_{10} respect C_3H_8 molecules together with the lack of stabilizing interactions between the alkyl chains of the gas and those of the walls of **1** (which do operate in **2** and **3**), which starts to have a non-negligible effect at the adsorption

Journal Name

ARTICLE

process. In addition, the slope in the C_2H_6, C_3H_8 and n-C_4H_{10} adsorption isotherms, especially the two latter, becomes much steeper (Fig. 5), which is a clear marker of a stronger affinity between larger hydrocarbons and the pore surface in **1**-**3**. Interestingly, C_2H_6/CH_4 and C_3H_8/CH_4 adsorption ratios, that is ideal selectivities, at 1 bar (Fig. 5) also follow the sequence **1** (3.69 and 4.29) < **2** (4.45 and 5.57) < **3** (4.51 and 5.64), suggesting that the larger is the alkyl group decorating the MOF (**1** < **2** < **3**), the larger is the separation equilibrium

between methane and the other hydrocarbon in the binary mixture.

The adsorption capabilities of **1**-**3** for olefins, C_2H_4 and C_3H_6, were also evaluated and are gathered, together with paraffins, in Fig. S11. The C_2H_4 adsorption isotherms for all three compounds are identical to the C_2H_6 ones. In turn, the amounts of C_3H_6 adsorbed by **1**-**3** are significantly higher than those observed in the case of C_3H_8, which may be due to the stronger interaction of the π-bonding orbital of C_3H_6 with open metal sites and its smaller kinetic diameter.[39]
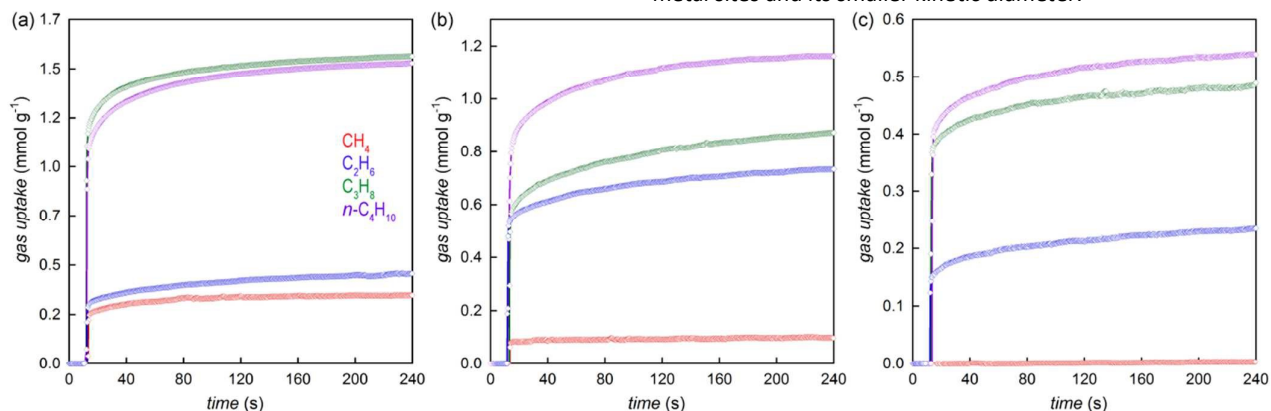

Fig. 6. Adsorption kinetic profiles of CH_4 (red), C_2H_6 (blue), C_3H_8 (green) and C_4H_{10} (purple) for compounds **1** (a), **2** (b) and **3** (c) at 273 K.

In view of the results shown in Fig. 5, and aiming at further confirming the effect of the increasing size of the alkyl chains in this new family of isoreticular MOFs in the adsorptive properties, kinetics adsorption of CH_4, C_2H_6, C_3H_8 and n-C_4H_{10} were performed (Fig. 6), which assess how fast hydrocarbons are adsorbed. A non-negligible impact on the kinetics adsorption was observed for the different adsorbates as we move from **1** to **3**. The adsorbed amount of n-C_4H_{10} with respect to C_3H_8 changes from being almost equal for **1,** to be significantly higher in **2**, as consequence of the higher number of aliphatic carbons able to interact with n-C_4H_{10}. However, these amounts tend to be similar in the case of **3**, probably due to the smaller window size of the MOF. Noteworthy, the adsorbed amount of C_2H_6 with respect to CH_4 shows a considerable increase as we move in the series **1**-**3**. Thus, the larger the alkyl side chain in the surface of the pores (**1** < **2** < **3**), the lower the amount of CH_4 adsorbed by the MOF. This is especially relevant for **3**, where CH_4 hardly adsorbs. These results (Fig. 6) further confirm the trend observed in the adsorption isotherms (Fig. 5) and even suggest higher mixture selectivities for methane respect other light hydrocarbons present in natural gas. Finally, the adsorption isotherm measurements collected in Fig. S11 also showed a certain selectivity for C_3H_6 *vs.* C_3H_8. Therefore, the kinetic adsorption of C_3H_6 was also evaluated and compared with that of C_3H_8. However, even if Fig. S12 shows a higher adsorption of C_3H_6 (especially for compound **2**), this small selectivity is not reflected on the time required to adsorb both gases in the kinetic experiments and does not allow to predict a successful separation and thus, breakthrough experiments were not carried out for these gases. The different experimental

conditions used in the adsorption isotherms (long waiting times until reach equilibrium) and the kinetics adsorption experiments (these experiment only measure the very beginning of the adsorption event) are at the origin of the apparent divergences observed on the adsorbed amounts between both experiments.
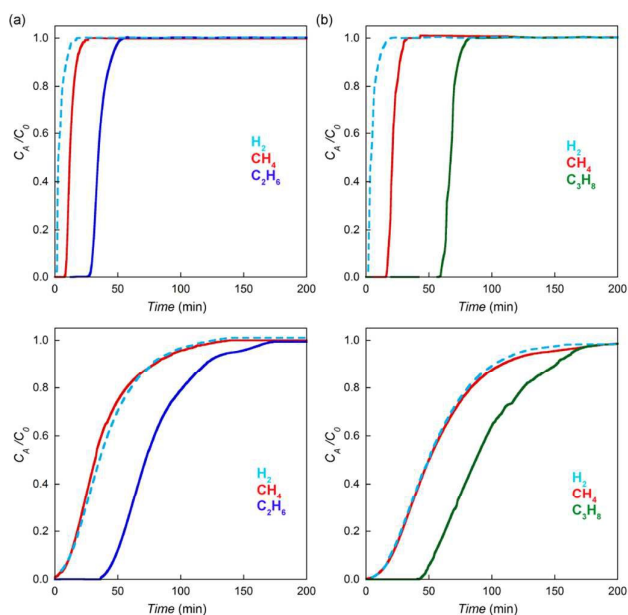

Fig. 7. Experimental column breakthrough curves for (a) CH_4/C_2H_6 (75:25, v/v) and (b) CH_4/C_3H_6 (75:25, v/v) gas mixtures measured at 298 K and 1 bar in a column using **1** (top) and **3** (bottom) as stationary phases. The total gas flow is 2 cm³ min⁻¹ in each case. H_2 was used as reference gas.

Overall, these results indicate that even if the pore window is key to explain the trend **1** > **2** > **3** in the adsorption capacities of this family, side-chain interactions between alkyl groups from both, gases and MOF walls, lie at the origin of their different selectivities. The very different uptake results for **1**-**3** clearly evidence that playing with the 'pore-limiting diameter' concept, through the increase the length of aliphatic side chains residing in the pores, does not only modify the sorption capacity of a given material but, more importantly, it may also affect kinetics of adsorption, which is of paramount relevance in order to perform separations in standard-flow conditions at industry.

In light of the results above, to investigate the practical separation performance of this family as well as to confirm the validity of our approach to tune the MOF selectivities, breakthrough experiments were carried out at 298 K and 1 bar for binary mixtures of CH_4/C_2H_6 (75/25) and CH_4/C_3H_8 (75/25) using packed columns (*ca.* 1 g) of **1** and **3** (Fig. 7) as stationary phases and a total gas flow of 2 cm^3/min. H_2, is used as internal reference gas because it does not adsorb under these conditions. In this way we can track the flow dispersion through the column.[68] CH_4 for sample **3** breaks at the same time as H_2, following the same profile (Fig. 7, bottom) and indicating non-uptake of CH_4 on this material. In contrast, C_2H_6 and C_3H_8 break much later, suggesting an almost infinite selectivity for the C_2H_6/CH_4 and C_3H_8/CH_4 separation. In case of **1**, CH_4 breaks later than H_2 (Fig. 7, top), suggesting a quantitative CH_4 adsorption and pointing towards a reduction of the selectivity for separating C_2H_6/CH_4 and C_3H_8/CH_4 mixtures. The lower slope of the breakthrough profile of **3** respect **1** can be attributed to the different flow regime through the bed. In the case of compound **1**, it is closer to a plug flow than in the case of compound **3**. In order to measure the non-ideality of the flows, we use H_2 as internal reference since H_2 is not adsorbed at this conditions and the profile of the H_2 flow is due to the dispersion of the bed. As it can be seen in Fig. 7, the fluid-dynamics are different in both beds but the retention times are reliable as H_2 is used as internal reference. Overall, as expected from the kinetic measurements, better separations of CH_4 from C_3H_8 and, especially, from C_2H_6 were observed for compound **3**. Yet, the differences in the C_3H_8–CH_4 and C_2H_6–CH_4 retention times were increased by *ca.* 5 and 30 min, respectively.

Conclusions

In summary, we have reported a unique family of robust, cheap and easy to prepare in large-scale isoreticular MOFs. These porous materials, showing overall good results in gas adsorption and separation, were prepared rationally from oxamidato ligands derived from the natural amino acids *L*-alanine, *L*-valine and *L*-leucine. Moreover, they offer the perfect playground to study how tuning of the length of the alkyl residues present in the channels of the MOFs modifies the gas adsorption capacities and selectivities towards different sized hydrocarbons. Overall, we observed that the higher was the length of the alkyl residue decorating the MOF

walls, the lesser was the affinity towards methane. As a consequence, we were able to control the kinetic adsorption selectivity of methane versus other light hydrocarbons present in natural gas, offering new rational ways for its purification.
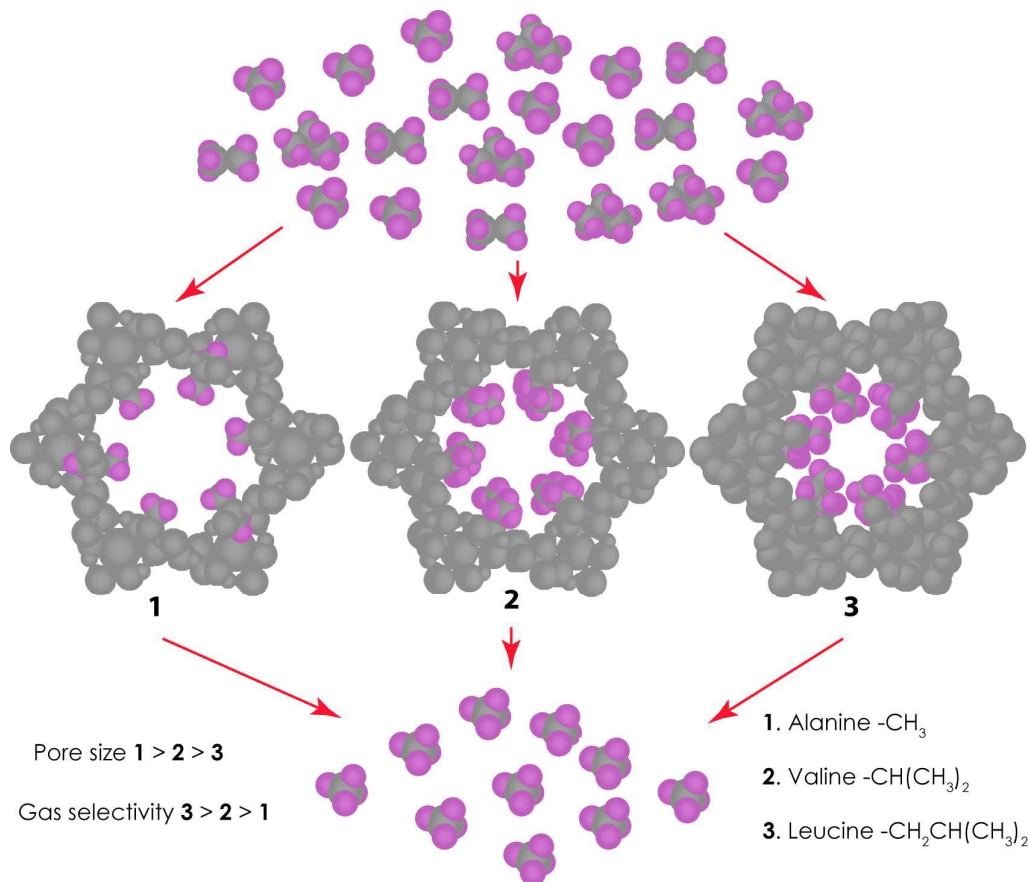
Acknowledgements

Notes and references

1 S. Matar and L. F. Hatch, in *Chemistry of Petrochemical Processes*, Elsevier, 2001, pp. 1–28.
2 G. A. Olah and Á. Molnár, *Hydrocarbon Chemistry*, John Wiley & Sons, Inc., Hoboken, NJ, USA, 2003.
3 M. Beckner and A. Dailly, *Appl. Energy*, 2015, **149**, 69–74.
4 A. Van Miltenburg, W. Zhu, F. Kapteijn and J. A. Moulijn, *Chem. Eng. Res. Des.*, 2006, **84**, 350–354.
5 X. Y. Chen, H. Vinh-Thang, A. A. Ramirez, D. Rodrigue and S. Kaliaguine, *RSC Adv.*, 2015, **5**, 24399–24448.
6 H. Wu, Q. Gong, D. H. Olson and J. Li, *Chem. Rev.*, 2012, **112**, 836–868.
7 S. Kitagawa and R. Matsuda, *Coord. Chem. Rev.*, 2007, **251**, 2490–2509.
8 G. Férey, *Chem. Soc. Rev.*, 2008, **37**, 191–214.
9 J. R. Long and O. M. Yaghi, *Chem. Soc. Rev.*, 2009, **38**, 1213–4.
10 O. K. Farha and J. T. Hupp, *Acc. Chem. Res.*, 2010, **43**, 1166–1175.
11 H. Furukawa, K. E. Cordova, M. O'Keeffe and O. M. Yaghi, *Science*, 2013, **341**, 974.
12 M. Pan, X.-M. Lin, G.-B. Li and C.-Y. Su, *Coord. Chem. Rev.*, 2011, **255**, 1921–1936.
13 T. Grancha, J. Ferrando-Soria, M. Castellano, M. Julve, J. Pasán, D. Armentano and E. Pardo, *Chem. Commun.*, 2014, **50**, 7569–7585.
14 Y. Cui, B. Li, H. He, W. Zhou, B. Chen and G. Qian, *Acc. Chem. Res.*, 2016, **49**, 483–493.
15 L. Fu, Y. Liu, M. Pan, X.-J. Kuang, C. Yan, K. Li, S.-C. Wei and C.-Y. Su, *J. Mater. Chem. A*, 2013, **1**, 8575.
16 M. Eddaoudi, *Science*, 2002, **295**, 469–472.
17 H. Furukawa, Y. B. Go, N. Ko, Y. K. Park, F. J. Uribe-Romo, J. Kim, M. O'Keeffe and O. M. Yaghi, *Inorg. Chem.*, 2011, **50**, 9147–9152.
18 R.-B. Lin, T.-Y. Li, H.-L. Zhou, C.-T. He, J.-P. Zhang and X.-M. Chen, *Chem. Sci.*, 2015, **6**, 2516–2521.
19 M. Kobalz, J. Lincke, K. Kobalz, O. Erhart, J. Bergmann, D. Lässig, M. Lange, J. Möllmer, R. Gläser, R. Staudt and H. Krautscheid, *Inorg. Chem.*, 2016, **55**, 3030–3039.

20 I. Spanopoulos, C. Tsangarakis, E. Klontzas, E. Tylianakis, G. Froudakis, K. Adil, Y. Belmabkhout, M. Eddaoudi and P. N. Trikalitis, *J. Am. Chem. Soc.*, 2016, **138**, 1568–1574.

21 M. G. Goesten, F. Kapteijn and J. Gascon, *CrystEngComm*, 2013, **15**, 9249–9257.

22 L. Carlucci, G. Ciani and D. M. Proserpio, in *Making Crystals by Design*, Wiley-VCH Verlag GmbH & Co. KGaA, Weinheim, Germany, 2007, pp. 58–85.

23 T. Grancha, M. Mon, J. Ferrando-Soria, D. Armentano and E. Pardo, *Cryst. Growth Des.*, 2016, **16**, 5571–5578.

24 W. M. Bloch, A. Burgun, C. J. Coghlan, R. Lee, M. L. Coote, C. J. Doonan and C. J. Sumby, *Nat. Chem.*, 2014, **6**, 906–912.

25 M. Mon, A. Pascual-Álvarez, T. Grancha, J. Cano, J. Ferrando-Soria, F. Lloret, J. Gascon, J. Pasán, D. Armentano and E. Pardo, *Chem. Eur. J.*, 2016, **22**, 539–545.

26 S. Yang, J. Sun, A. J. Ramirez-Cuesta, S. K. Callear, W. I. F. David, D. P. Anderson, R. Newby, A. J. Blake, J. E. Parker, C. C. Tang and M. Schröder, *Nat. Chem.*, 2012, **4**, 887–894.

27 Y. Peng, V. Krungleviciute, I. Eryazici, J. T. Hupp, O. K. Farha and T. Yildirim, *J. Am. Chem. Soc.*, 2013, **135**, 11887–11894.

28 Z. R. Herm, E. D. Bloch and J. R. Long, *Chem. Mater.*, 2014, **26**, 323–338.

29 Z. Bao, G. Chang, H. Xing, R. Krishna, Q. Ren and B. Chen, *Energy Environ. Sci.*, 2016.

30 E. López-Maya, C. Montoro, L. M. Rodríguez-Albelo, S. D. Aznar Cervantes, A. A. Lozano-Pérez, J. L. Cenís, E. Barea and J. A. R. Navarro, *Angew. Chem., Int. Ed.*, 2015, **54**, 6790–6794.

31 J. E. Mondloch, M. J. Katz, W. C. Isley III, P. Ghosh, P. Liao, W. Bury, G. W. Wagner, M. G. Hall, J. B. DeCoste, G. W. Peterson, R. Q. Snurr, C. J. Cramer, J. T. Hupp and O. K. Farha, *Nat. Mater.*, 2015, **14**, 512–516.

32 F. Luo, C. Yan, L. Dang, R. Krishna, W. Zhou, H. Wu, X. Dong, Y. Han, T.-L. Hu, M. O'Keeffe, L. Wang, M. Luo, R.-B. Lin and B. Chen, *J. Am. Chem. Soc.*, 2016, **138**, 5678–5684.

33 S. Yang, X. Lin, W. Lewis, M. Suyetin, E. Bichoutskaia, J. E. Parker, C. C. Tang, D. R. Allan, P. J. Rizkallah, P. Hubberstey, N. R. Champness, K. Mark Thomas, A. J. Blake and M. Schröder, *Nat. Mater.*, 2012, **11**, 710–716.

34 T. M. McDonald, J. A. Mason, X. Kong, E. D. Bloch, D. Gygi, A. Dani, V. Crocellà, F. Giordanino, S. O. Odoh, W. S. Drisdell, B. Vlaisavljevich, A. L. Dzubak, R. Poloni, S. K. Schnell, N. Planas, K. Lee, T. Pascal, L. F. Wan, D. Prendergast, J. B. Neaton, B. Smit, J. B. Kortright, L. Gagliardi, S. Bordiga, J. A. Reimer and J. R. Long, *Nature*, 2015, **519**, 303–308.

35 C. Gücüyener, J. van den Bergh, J. Gascon and F. Kapteijn, *J. Am. Chem. Soc.*, 2010, **132**, 17704–17706.

36 Y. He, R. Krishna and B. Chen, *Energy Environ. Sci.*, 2012, **5**, 9107.

37 D. Peralta, G. Chaplais, A. Simon-Masseron, K. Barthelet, C. Chizallet, A.-A. Quoineaud and G. D. Pirngruber, *J. Am. Chem. Soc.*, 2012, **134**, 8115–8126.

38 E. D. Bloch, W. L. Queen, R. Krishna, J. M. Zadrozny, C. M. Brown and J. R. Long, *Science*, 2012, **335**, 1606–1610.

39 Y.-S. Bae, C. Y. Lee, K. C. Kim, O. K. Farha, P. Nickias, J. T. Hupp, S. T. Nguyen and R. Q. Snurr, *Angew. Chem., Int. Ed.*, 2012, **51**, 1857–1860.

40 S. J. Geier, J. a. Mason, E. D. Bloch, W. L. Queen, M. R. Hudson, C. M. Brown and J. R. Long, *Chem. Sci.*, 2013, **4**, 2054.

41 C. Yu, M. G. Cowan, R. D. Noble and W. Zhang, *Chem. Commun.*, 2014, **50**, 5745.

42 42 B. Li, Y. Zhang, R. Krishna, K. Yao, Y. Han, Z. Wu, D. Ma, Z. Shi, T. Pham, B. Space, J. Liu, P. K. Thallapally, J. Liu, M. Chrzanowski and S. Ma, *J. Am. Chem. Soc.*, 2014, **136**, 8654–8660.

43 P.-Q. Liao, W.-X. Zhang, J.-P. Zhang and X.-M. Chen, *Nat. Commun.*, 2015, **6**, 8697.

44 A. H. Assen, Y. Belmabkhout, K. Adil, P. M. Bhatt, D.-X. Xue, H. Jiang and M. Eddaoudi, *Angew. Chem., Int. Ed.*, 2015, **54**, 14353–14358.

45 D.-X. Xue, Y. Belmabkhout, O. Shekhah, H. Jiang, K. Adil, A. J. Cairns and M. Eddaoudi, *J. Am. Chem. Soc.*, 2015, **137**, 5034–5040.

46 A. Cadiau, K. Adil, P. M. Bhatt, Y. Belmabkhout and M. Eddaoudi, *Science*, 2016, **353**, 137–140.

47 T. Grancha, J. Ferrando-Soria, H.-C. Zhou, J. Gascon, B. Seoane, J. Pasán, O. Fabelo, M. Julve and E. Pardo, *Angew. Chem., Int. Ed.*, 2015, **54**, 6521–6525.

48 X. Zhao, J. G. Bell, S.-F. Tang, L. Li and K. M. Thomas, *J. Mater. Chem. A*, 2016, **4**, 1353–1365.

49 M.-C. Dul, E. Pardo, R. Lescouëzec, Y. Journaux, J. Ferrando-Soria, R. Ruiz-García, J. Cano, F. Lloret, D. Cangussu, C. L. M. Pereira, H. O. Stumpf, J. Pasán and C. Ruiz-Pérez, *Coord. Chem. Rev.*, 2010, **254**, 2281–2296.

50 T. Grancha, J. Ferrando-Soria, J. Cano, F. Lloret, M. Julve, G. De Munno, D. Armentano and E. Pardo, *Chem. Commun.*, 2013, **49**, 5942–4.

51 T. Grancha, J. Ferrando-Soria, J. Cano, P. Amorós, B. Seoane, J. Gascon, M. Bazaga-García, E. R. Losilla, A. Cabeza, D. Armentano and E. Pardo, *Chem. Mater.*, 2016, **28**, 4608–4615.

52 M. Mon, J. Ferrando-Soria, T. Grancha, F. R. Fortea-Pérez, J. Gascon, A. Leyva-Pérez, D. Armentano and E. Pardo, *J. Am. Chem. Soc.*, 2016, **138**, 7864–7867.

53 M. Mon, F. Lloret, J. Ferrando-Soria, C. Martí-Gastaldo, D. Armentano and E. Pardo, *Angew. Chem., Int. Ed.*, 2016, **55**, 11167–11172.

54 M. O'Keeffe, M. A. Peskov, S. J. Ramsden and O. M. Yaghi, *Acc. Chem. Res.*, 2008, **41**, 1782–1789.

55 A. C. Sudik, A. P. Côté and O. M. Yaghi, *Inorg. Chem.*, 2005, **44**, 2998–3000.

56 M. F. De Lange, T. J. H. Vlugt, J. Gascon and F. Kapteijn, *Microporous Mesoporous Mater.*, 2014, **200**, 199–215.

57 R. J. Dombrowski, C. M. Lastoskie and D. R. Hyduke, *Colloids Surfaces A Physicochem. Eng. Asp.*, 2001, **187–188**, 23–39.

58 A. L. Myers and J. M. Prausnitz, *AIChE J.*, 1965, **11**, 121–127.

59 R. Krishna and J. R. Long, *J. Phys. Chem. C*, 2011, **115**, 12941–12950.

60 S. Horike, Y. Inubushi, T. Hori, T. Fukushima and S. Kitagawa, *Chem. Sci.*, 2012, **3**, 116–120.

61 J. Duan, M. Higuchi, S. Horike, M. L. Foo, K. P. Rao, Y. Inubushi, T. Fukushima and S. Kitagawa, *Adv. Funct. Mater.*, 2013, **23**, 3525–3530.

62 J. W. Yoon, J. S. Lee, S. Lee, K. H. Cho, Y. K. Hwang, M. Daturi, C.-H. Jun, R. Krishna and J.-S. Chang, *Chem. Eur. J.*, 2015, **21**, 18431–18438.

63 A. M. Plonka, X. Chen, H. Wang, R. Krishna, X. Dong, D. Banerjee, W. R. Woerner, Y. Han, J. Li and J. B. Parise, *Chem. Mater.*, 2016, **28**, 1636–1646.

64 L. H. Wee, M. Meledina, S. Turner, G. Van Tendeloo, K. Zhang, L. M. Rodriguez-Albelo, A. Masala, S. Bordiga, J. Jiang, J. A. R. Navarro, C. E. A. Kirschhock and J. A. Martens, *J. Am. Chem. Soc.*, 2017, jacs.6b10768.

65 K. Liu, D. Ma, B. Li, Y. Li, K. Yao, Z. Zhang, Y. Han and Z. Shi, *J. Mater. Chem. A*, 2014, **2**, 15823–15828.

66 S. N. Talapaneni, D. Kim, G. Barin, O. Buyukcakir, S. H. Je and A. Coskun, *Chem. Mater.*, 2016, **28**, 4460–4466.

67 A. Schneemann, E. D. Bloch, S. Henke, P. L. Llewellyn, J. R. Long and R. A. Fischer, *Chem. Eur. J.*, 2015, **21**, 18764–18769.

68 V. Safarifard, S. Rodríguez-Hermida, V. Guillerm, I. Imaz, M. Bigdeli, A. Azhdari Tehrani, J. Juanhuix, A. Morsali, M. E. Casco, J. Silvestre-Albero, E. V. Ramos-Fernandez and D. Maspoch, *Cryst. Growth Des.*, 2016, **16**, 6016–6023.

Tuning the Selectivity of Light Hydrocarbons in Natural Gas in a Family of Isoreticular MOFs

Thais Grancha, Marta Mon, Jesús Ferrando-Soria,* Jorge Gascon, Beatriz Seoane, Enrique V. Ramos-Fernandez, Donatella Armentano,* and Emilio Pardo*

Pore size **1** > **2** > **3**

Gas selectivity **3** > **2** > **1**

1. Alanine -CH_3

2. Valine -$CH(CH_3)_2$

3. Leucine -$CH_2CH(CH_3)_2$

Kinetic adsorption selectivity of methane versus other light hydrocarbons, present in natural gas, is tuned in a rationally synthesized family of isoreticular MOFs.